Int. J. Nonlinear Anal. Appl. 15 (2024) 7, 153–166
ISSN: 2008-6822 (electronic)
http://dx.doi.org/10.22075/ijnaa.2022.28541.3922

Design of a novel four-feed dual-band microstrip antenna with pure circular polarization and analysis of circular polarization parameters

Saeed Komeylian[a], Majid Tayarani[a,*], Seyed Hassan Sedighy[b]

[a]Department of Electrical Engineering, Iran University of Science and Technology, Tehran 16846-13114, Iran

[b]School of New Technologies, Iran University of Science and Technology, Tehran 16846-13114, Iran

(Communicated by Madjid Eshaghi Gordji)

Abstract

In this study, a novel dual-band multiple-feed microstrip antenna is introduced for GNSS applications. The proposed antenna has a compact size of 1548 mm^2 and counts as a low-cost, low-profile antenna. The mathematical equations of multiple-feed configuration are driven to analyze circular polarization (CP) generation and find the effective parameters on CP value. It is shown that for an n-feed symmetric antenna, the phase shift of $\frac{2\pi}{n}$ between ports leads to pure CP, regardless of the electrical field pattern. However, if the first feed electric field has equal value in the x and y direction and also 90° phase shift, the CP value is increased. A symmetric four-feed configuration is employed on the antenna to generate CP. Also, fractal circular rings and perturbing sectors are applied to miniaturize the antenna and improve the CP value. Numerical simulation shows that all feeding network requirements are met and the phase shift is satisfied at both frequencies by using the coupler technique. Furthermore, results show desirable band width of 48 MHz and 60 MHz and high front to back ratio of 16.1 and 14 at f_1=1.227 GHz and f_2=1.575 GHz, respectively. The axial ratio (AR) beam-width at both frequencies is more than 66°.

Keywords: Axial Ratio, Circular Polarization, Dual-band, GNSS, Multiple-Feed
2020 MSC: 62F35, 74K10

1 Introduction

Microstrip patch antennas are widely used due to their compact size, low-cost and easy fabrication. However, microstrip antenna has some drawbacks such as narrow band-width and low gain [14]. Consequently, several new techniques in the antenna design process are applied to improve the performance [16, 7, 15].

Type of polarization is an important factor for the antenna application. In linear polarization, transmit and received antenna have to be accurately aligned. However, circularly polarized antenna is able to receive signals regardless of transmit and received antenna orientation. As a result, multipath elimination is the most important feature for antenna with CP [15, 20].

*Corresponding author
Email addresses: komeylian.official@gmail.com (Saeed Komeylian), m_Tayarani@iust.ac.ir (Majid Tayarani), sedighy@iust.ac.ir (Seyed Hassan Sedighy)

Received: September 2022 *Accepted:* November 2022

Feed type has considerable effect on the CP production. Single feed configuration leads to easy design and fabrication, however, some perturbations are needed in the structure of antenna with respect to the feed to excite orthogonal modes [19]. Perturbations include slits [8, 1], cutting annular rings [3, 22, 13, 17, 6, 18, 21], cross shaped slots [5, 23, 9], Y shaped slots [12, 23, 4], and truncating corners [2, 1, 16, 12].

The CP quality is enhanced using multiple-feed configuration while they have large size and increase the antenna size [3, 6, 12, 10]. There are some methods of decreasing the antenna size such as fractal structures which increase the current length and cause a shift in resonant frequency. Thus, working at desire frequency leads to the size reduction of antenna [11].

In this study, a multiple-feed dual-band antenna with CP is proposed. The proposed antenna operates at GPS L1 (1575 MHz) and L2 (1227 MHz), GLONASS G1 (1602 MHz) and G3 (1207 MHz), Galileo E1 (1589 MHz), E2 (1561 MHz) and E5b (1207 MHz) bands. The four-feed configuration is designed so that prevent the antenna size increment. Also, fractal structure is applied to miniaturize the antenna. In the following sections, the theory of CP production and effective parameters on CP are evaluated. Furthermore, the antenna design process, feeding network requirements and Numerical simulation results are stated.

2 Analysis of electrical field for circular polarization of multiple-feed antenna

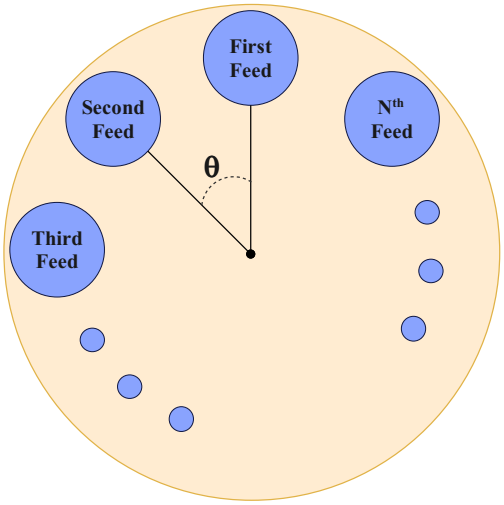

Figure 1: Schematic of n-feed configuration

The electric field created by feeding port 1 in the z direction is stated as (2.1).

$$E_1 = \begin{bmatrix} e_{0x} \\ e_{0y} \\ e_{0z} \end{bmatrix} \tag{2.1}$$

The field created by the second feeding port is implied as (2.2). Considering the symmetric arrangement of feed location, the electric field resulting from E_2 is similar to E_1, with the difference of θ. The T matrix represents rotation around the Z axis and is shown as (2.3). The time delay between excitation of the second port and first port is considered as φ.

$$E_2 = e^{-j\varphi}\,[T(\theta)] \begin{bmatrix} e_{0x} \\ e_{0y} \\ e_{0z} \end{bmatrix} \tag{2.2}$$

$$[T(\theta)] = \begin{bmatrix} \cos\theta & -\sin\theta & 0 \\ \sin\theta & \cos\theta & 0 \\ 0 & 0 & 1 \end{bmatrix} \tag{2.3}$$

Similarly, the electric field caused by the N^{th} feeding port is calculated as (2.4).

$$E_n = e^{-j(n-1)\varphi}\left[T\left((n-1)\theta\right)\right]\begin{bmatrix} e_{0x} \\ e_{0y} \\ e_{0z} \end{bmatrix} \tag{2.4}$$

The total electrical field on the Z axis is obtained by summation of the fields of all N ports as written in (2.5).

$$E_{total} = \sum_{i=1}^{n} E_i = \left(\sum_{i=0}^{n-1} e^{-ji\varphi}\left[T(i\theta)\right]\right)\begin{bmatrix} e_{0x} \\ e_{0y} \\ e_{0z} \end{bmatrix} \tag{2.5}$$

The T matrix is written as (2.6) for simpler calculations.

$$[T(\theta)] = [F(\theta)] + [F(-\theta)]^T \tag{2.6}$$

The F matrix is defined as (2.7):

$$[F(\theta)] \triangleq \frac{1}{2}\begin{bmatrix} e^{j\theta} & je^{j\theta} & 0 \\ -je^{j\theta} & e^{j\theta} & 0 \\ 0 & 0 & 1 \end{bmatrix} \tag{2.7}$$

Rewriting the total electric field in terms of matrix F resulted in (2.8).

$$E_{total} = \sum_{i=1}^{n} E_i = \left(\sum_{i=0}^{n-1} e^{-ji\varphi}\left([F(i\theta)] + [F(-i\theta)]^T\right)\right)\begin{bmatrix} e_{0x} \\ e_{0y} \\ e_{0z} \end{bmatrix} \tag{2.8}$$

The first term of the series is calculated from (2.9).

$$\sum_{i=0}^{n-1} e^{-ji\varphi}\left[F(i\theta)\right] = \frac{1}{2}\sum_{i=0}^{n-1}\begin{bmatrix} e^{ji\alpha} & \frac{-e^{ji\alpha}}{j} & 0 \\ \frac{e^{ji\alpha}}{j} & e^{ji\alpha} & 0 \\ 0 & 0 & e^{-ji\varphi} \end{bmatrix} \tag{2.9}$$

where α is defined as (2.10).

$$\alpha \triangleq -\varphi + \theta \tag{2.10}$$

From geometric series relationship, (2.11) can be written.

$$\sum_{i=0}^{n-1}\left(e^{ji\alpha}\right) = \frac{1-e^{jn\alpha}}{1-e^{j\alpha}}. \tag{2.11}$$

In the above relationship, if $\alpha = 0$, the value of the series will be "n", which is equal to its limit when $\alpha \to 0$. Therefore, the first term of the electric field series is calculated as (2.12).

$$\sum_{i=0}^{n-1} e^{-ji\varphi}\left[F(i\theta)\right] = \frac{1}{2}\frac{1-e^{jn\alpha}}{1-e^{j\alpha}}\begin{bmatrix} 1 & j & 0 \\ -j & 1 & 0 \\ 0 & 0 & \frac{1-e^{-jn\varphi}}{1-e^{-j\varphi}}\frac{1-e^{j\alpha}}{1-e^{jn\alpha}} \end{bmatrix} \tag{2.12}$$

Using equations (2.7) to (2.12) yields the total electric field as (2.13).

$$E_{total} = \left(\sum_{i=0}^{n-1} e^{-ji\varphi}([F(i\theta)] + [F(-i\theta)]^T)\right)\begin{bmatrix} e_{0x} \\ e_{0y} \\ e_{0z} \end{bmatrix} = \frac{1}{2}\begin{bmatrix} ue_{0x} - ve_{0y} \\ ve_{0x} + ue_{0y} \\ 2\frac{1-e^{-jn\varphi}}{1-e^{-j\varphi}}e_{0z} \end{bmatrix} = \begin{bmatrix} e_x \\ e_y \\ e_z \end{bmatrix} \tag{2.13}$$

where u and v are defined as (2.14) and (2.15).

$$u \triangleq \frac{1-e^{jn\alpha}}{1-e^{j\alpha}} + \frac{1-e^{-jn\beta}}{1-e^{-j\beta}} \tag{2.14}$$

$$v \triangleq -j\frac{1-e^{jn\alpha}}{1-e^{j\alpha}} + j\frac{1-e^{-jn\beta}}{1-e^{-j\beta}} \tag{2.15}$$

Also, β is implied as (2.16).

$$\beta \triangleq -\varphi - \theta \tag{2.16}$$

Finally, the components of the electric field in the direction of X, Y and Z are written as (2.17), (2.18) and (2.19), respectively.

$$e_x = ue_{0x} - ve_{0y} = \frac{1}{2}\left(\frac{1-e^{jn\alpha}}{1-e^{j\alpha}} + \frac{1-e^{-jn\beta}}{1-e^{-j\beta}}\right)e_{0x} + j\frac{1}{2}\left(\frac{1-e^{jn\alpha}}{1-e^{j\alpha}} - \frac{1-e^{-jn\beta}}{1-e^{-j\beta}}\right)e_{0y} \tag{2.17}$$

$$e_y = ve_{0x} + ue_{0y} = -j\frac{1}{2}\left(\frac{1-e^{jn\alpha}}{1-e^{j\alpha}} - \frac{1-e^{-jn\beta}}{1-e^{-j\beta}}\right)e_{0x} + \frac{1}{2}\left(\frac{1-e^{jn\alpha}}{1-e^{j\alpha}} + \frac{1-e^{-jn\beta}}{1-e^{-j\beta}}\right)e_{0y} \tag{2.18}$$

$$e_z = \frac{1-e^{-jn\varphi}}{1-e^{-j\varphi}}e_{0z} \tag{2.19}$$

The decomposition of the electric field into right-hand and left-hand parts is implied as (2.20) and (2.21).

$$e_x = R + L \tag{2.20}$$

$$e_y = jR - jL. \tag{2.21}$$

Therefore, the right-handed electric field is calculated from (2.22).

$$R = \frac{e_x - je_y}{2} = \frac{1-e^{-jn\beta}}{1-e^{-j\beta}}\left(e_{0x} - je_{0y}\right) \tag{2.22}$$

Similarly, the left-handed electric field is obtained from (2.23).

$$L = \frac{e_x + je_y}{2} = \frac{1-e^{jn\alpha}}{1-e^{j\alpha}}\left(e_{0x} + je_{0y}\right) \tag{2.23}$$

The polar form of right-handed and left-handed electric fields are stated as (2.24) and (2.25), respectively.

$$R = |R|\, e^{j\varphi_R} \tag{2.24}$$

$$L = |L|\, e^{j\varphi_L}. \tag{2.25}$$

In this study, the magnitude of the right-handed and left-handed fields are of interest. The magnitude of Right-handed electric field is written in terms of f and g functions, as (2.26).

$$|R| = f(\mathrm{r_0}, \mathrm{p}, \mathrm{q}, \mathrm{n})g(n, \beta) \tag{2.26}$$

where the function g is defined as (2.27),

$$g(n, \beta) = \left|\frac{\sin\frac{n\beta}{2}}{n\sin\frac{\beta}{2}}\right| \tag{2.27}$$

and the function f is defined as (2.28):

$$f(r_0, p, q, n) = n\sqrt{|e_{0x}|^2 + |e_{0y}|^2 + j(e_{0x}e^*{}_{0y} - e^*{}_{0x}e_{0y})} = nr_0\sqrt{1 + \frac{2p\sin q}{1+p^2}} \tag{2.28}$$

r_0, p and q are represented as the f function parameters, depend on the electric field of the first feed on the Z axis. p and q are defined in polar coordinates as (2.29),

$$pe^{jq} = \frac{e_{0y}}{e_{0x}} \tag{2.29}$$

Also, r_0 is stated as (2.30),

$$r_0 = \sqrt{|e_{0x}|^2 + |e_{0y}|^2}. \tag{2.30}$$

Similarly, the magnitude of the left-handed electric field is written as (2.31).

$$|L| = f(\mathrm{r_0, p, -q, n})g(n, \alpha). \tag{2.31}$$

As mentioned in (2.26), R is obtained by product of f and g functions. So maximizing f and g functions leads to maximum value of R. The maximum value of f function is obtained by solving the system of equations stated in (2.32), which results in $p = 1$ and $q = 90°$. This is clearly illustrated by plotting the contour of normalized f function ($f_{nr_0} = \frac{f}{nr_0}$) versus different p and q in figure 2.

$$\begin{cases} \frac{\partial f(r_0,p,q,n)}{\partial p} = 0 \\ \frac{\partial f(r_0,p,q,n)}{\partial q} = 0 \end{cases} \tag{2.32}$$

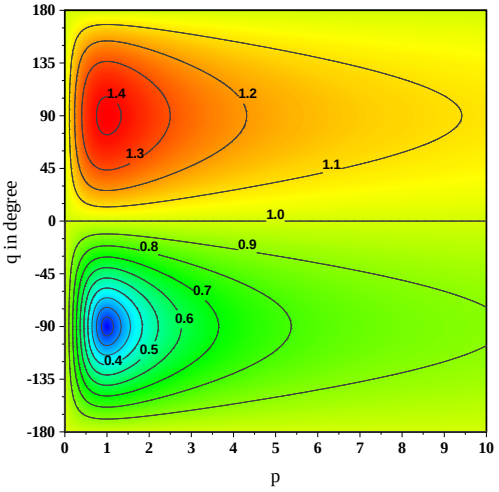

Figure 2: The normalized f function behavior towards p and q

The g function states the spatial angle and temporal angle differences for the $(n-1)$th and nth feeding port. Due to spatial and time symmetry of feeding ports, θ is obtained from (2.33).

$$\theta = \frac{2\pi}{n}. \tag{2.33}$$

Figure 3 depicts the g function value versus β for different number of feeding ports. As clearly shown, the maximum value of g is occurred at β=0. Therefore, the value of φ is set to $-\theta$ as shown in (2.34).

$$\varphi = -\frac{2\pi}{n}. \tag{2.34}$$

It is reminded that maximizing the g function leads to maximum value of R.

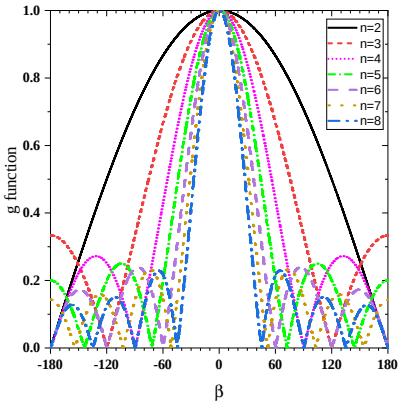

Figure 3: The g function behavior towards β and n

The polarization purity is evaluated by the axial ratio parameter, which is calculated from (2.35).

$$AR = \left| \frac{|R| + |L|}{|R| - |L|} \right| \tag{2.35}$$

Substituting the (2.26) and (2.31) in AR equation reveals (2.36). In the field of electromagnetic waves, AR is count as a very important parameter. As it is clear from (2.36), the AR value is equal or greater than one and the smaller it is, the higher CP purity is achieved. In the case of AR=1, the pure polarization is obtained. Obviously, if either R or L is zero, AR equals to 1.

$$\begin{aligned} AR(\mathrm{p,q,n},\alpha,\beta) &= \left| \frac{|f(\mathrm{r_0,p,q,n})g(n,\beta)| + |f(\mathrm{r_0,p,-q,n})g(n,\alpha)|}{|f(\mathrm{r_0,p,q,n})g(n,\beta)| - |f(\mathrm{r_0,p,-q,n})g(n,\alpha)|} \right| \\ &= \left| \frac{\left|\sqrt{1+p^2+2p\sin q}\right| \left|\sin\frac{n\beta}{2}\sin\frac{\alpha}{2}\right| + \left|\sqrt{1+p^2-2p\sin q}\right| \left|\sin\frac{\beta}{2}\sin\frac{n\alpha}{2}\right|}{\left|\sqrt{1+p^2+2p\sin q}\right| \left|\sin\frac{n\beta}{2}\sin\frac{\alpha}{2}\right| - \left|\sqrt{1+p^2-2p\sin q}\right| \left|\sin\frac{\beta}{2}\sin\frac{n\alpha}{2}\right|} \right| \end{aligned} \tag{2.36}$$

Figure 4 shows AR behavior towards n, α and β.

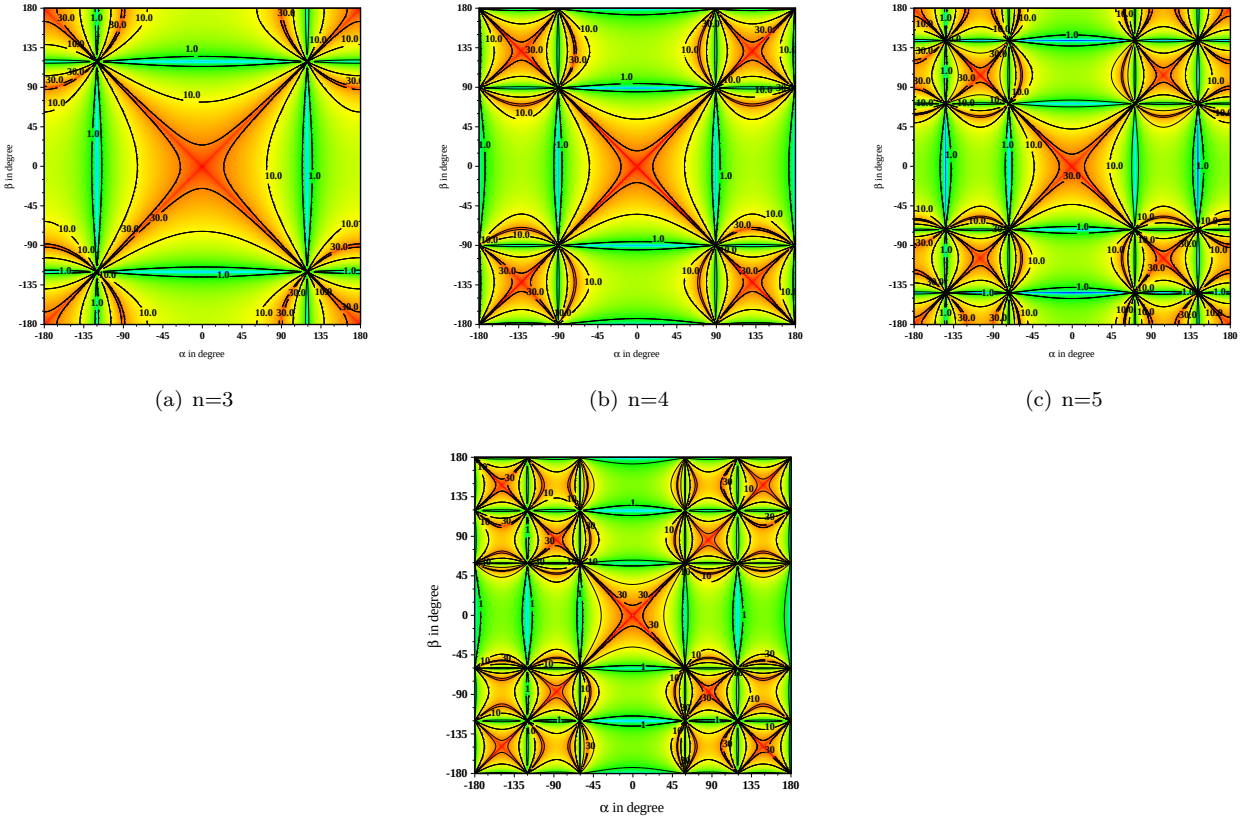

(a) n=3 (b) n=4 (c) n=5

(d) n=6

Figure 4: $AR(n,\alpha,\beta)$ $[dB]$ for LP

Several special cases are considered to simplify and evaluate CP behavior. For these cases AR equation is converted to (2.37). In other words, if the electric field of first feed is linear, AR is calculated from (2.37).

$$AR(\mathrm{n},\alpha,\beta) = \left| \frac{\left|\sin\frac{n\beta}{2}\sin\frac{\alpha}{2}\right| + \left|\sin\frac{\beta}{2}\sin\frac{n\alpha}{2}\right|}{\left|\sin\frac{n\beta}{2}\sin\frac{\alpha}{2}\right| - \left|\sin\frac{\beta}{2}\sin\frac{n\alpha}{2}\right|} \right| \tag{2.37}$$

The first case is $q = 0$. As can be seen in (2.37), the function AR for $q = 0$ is independent of p and r_0. It means that, if there is no phase difference between the x and y components of the electric field, the axial ratio is independent of their magnitude. The second case is $q = \pi$ which has the same behavior as $q = 0$ refer to (2.37). $p \to 0$ is considered as the third state. As can be seen, in this case, the value of AR is independent of q. The fourth case is $p \to \infty$ where the value of AR is independent of q, similar to the third case.

L and R function has the same subordination, while L is an α function, not a β one. At this state the α value is obtained from (2.38).

$$\alpha = -\varphi + \theta = \frac{2\pi}{n} + \frac{2\pi}{n} = \frac{4\pi}{n} \tag{2.38}$$

By setting $\alpha = \frac{4\pi}{n}$, for $n > 2$, the L function becomes zero according to equation (2.39).

$$|L| = f(\mathrm{r_0, p, -q, n})g(n, \frac{4\pi}{n}) = f(\mathrm{r_0, p, -q, n}) \left| \frac{\sin \frac{n\frac{4\pi}{n}}{2}}{n \sin \frac{\frac{4\pi}{n}}{2}} \right| = f(\mathrm{r_0, p, -q, n}) \left| \frac{\sin 2\pi}{n \sin \frac{2\pi}{n}} \right| = 0 \tag{2.39}$$

$$|R| = f(\mathrm{r_0, p, q, n})g(n, 0) = f(\mathrm{r_0, p, q, n}) = nr_0 \sqrt{1 + \frac{2p \sin q}{1 + p^2}} \tag{2.40}$$

Zero value of L function leads to AR=1 and thus pure right-handed circular polarization. It is noteworthy that R value depends on the electric field produced by the first feeding port. However, regardless of the feeding ports electric fields and thus R, pure right-handed circular polarization is achieved by adjusting the time phase shift value of the feeding ports excitation with the negative spatial phase shift of the feeding ports. In a similar way, the pure left-handed circular polarization is obtained.

3 Simulation Result

In this study, a new single-layer four feed dual-band GNSS antenna is designed to operate at resonant frequencies of 1.22 GHz and 1.575 GHz. The antenna geometry is depicted in Figure 5 . The geometric parameters of the designed antenna and their optimum values are presented in table 1.

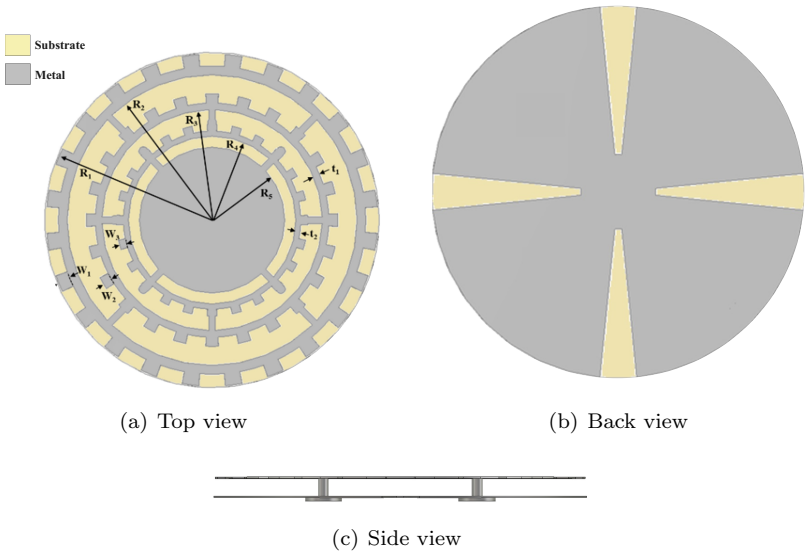

(a) Top view (b) Back view

(c) Side view

Figure 5: Geometry of the proposed antenna

Table 1: The geometric parameters

Geometric parameters	Value (mm)	Geometric parameters	Value (mm)
R_1	22.4	W_1	1.61
R_2	19.4	W_2	1.24
R_3	14.7	W_3	0.924
R_4	11.2	t_1	0.89
R_5	9.74	t_2	0.68

The feeding network is printed on a FR4 substrate with thickness of 2 mm and dielectric constant of 4.4. It consists of a coaxial prob, phase shifter and a 4-way power divider. The fabricated antenna and feed location on the patch are illustrated in Figure 6. As clearly shown feeds locations are symmetric.

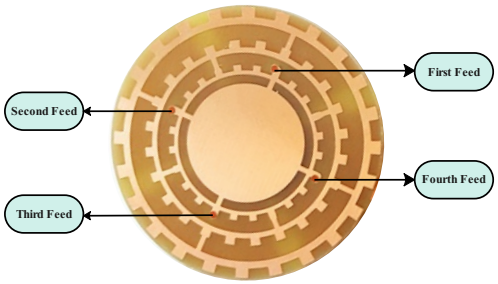

Figure 6: Fabricated antenna

3.1 Feeding network design

As shown in Figure 7, Feeds should be excited with 90° time delay to generate circular polarization according to the derived mathematical equations.

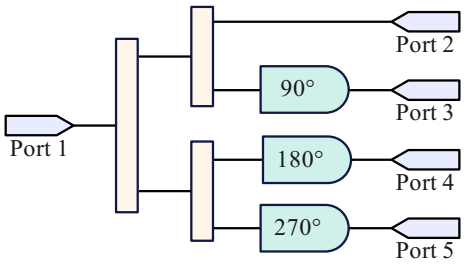

Figure 7: Schematic of feeding network with required time delay

In the design of the feeding network, there are standard requirements. The first requirement is to match input and output ports. It means that the return loss value of the input and output ports should be considered below -15 dB (for the input port, the safety margin of -20 dB is considered). Another requirement for the design of the feeding network is the input-to-output transfer coefficient, which is ideally -6 dB (full division of the input power into four output ports without any losses). In this study, the value of the transmission coefficient is considered at least -6.8 dB (equivalent to 0.8 dB path loss). Also, after counting the path losses, it is still necessary for the power in all output ports to be equal to each other. The other requirement in the design of the feeding network is the isolation of the four output ports from each other. Finally, the phase shift of the output ports must be 90° to produce circular polarization, which is also a requirement of the network design. In the presented design, in order to comply with the aforementioned restrictions, the following elements have been used:

- Transmission line: to produce a 90° phase shift between the output ports
- Narrowing transmission line: to adapt to the entry and exit
- Open circuit transmission line: to create matching impedance
- Connection element (4 ways): dividing the input signal into four parts (for four output ports)
- Coupler: To produce 90° phase shift at second resonant frequency
- Electrical resistance: to create isolation

The matching, isolation, transfer coefficient and phase difference of the designed feeding network are presented in Figures 8 to 11,respectively. Port 1 in following figures refers to input port and port 2 to port 5 implies the output ports.

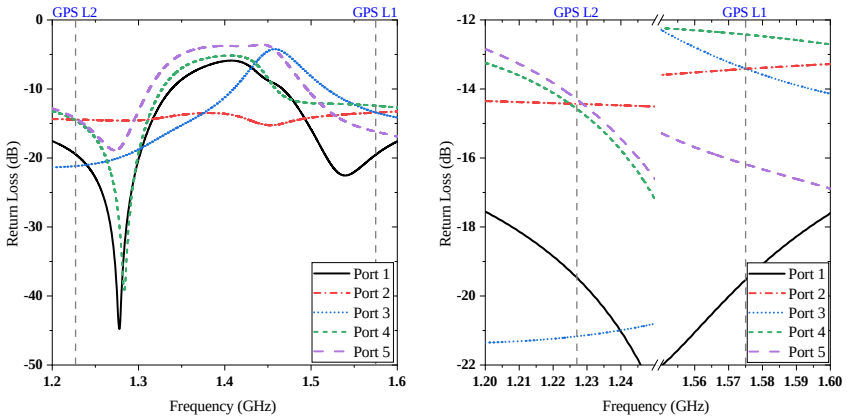

(a) General view (b) Magnified view

Figure 8: Matching of input and output ports

As shown in Figure 8, the return loss value of all input and output ports in the designed feeding network is below -12 dB and the matching conditions are satisfied.

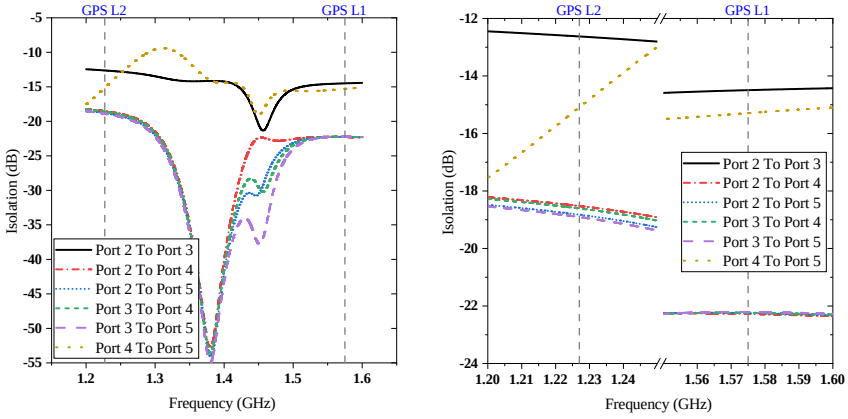

(a) General view (b) Magnified view

Figure 9: Isolation of output ports from each other

Figure 9 illustrates that the return loss of the antenna output ports relative to each other is below -12 dB. Hence output ports are isolated from each other.

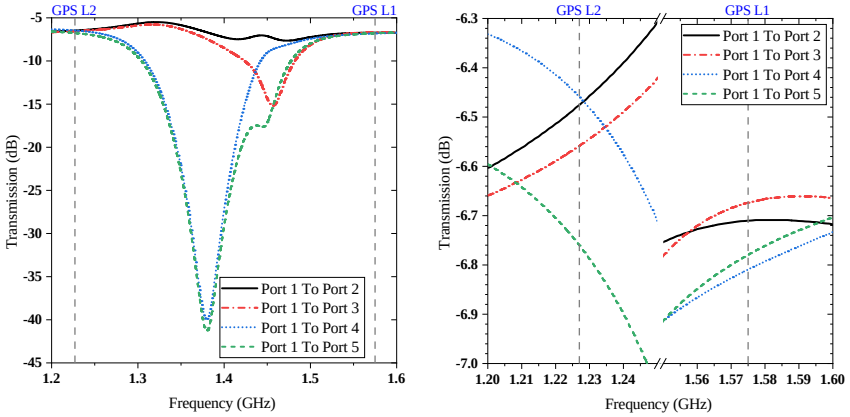

(a) General view (b) Magnified view

Figure 10: Input to output ports transfer coefficient

It is clear from Figure 10 that despite the use of low-cost FR4 substrate with high losses, the maximum path loss is about 0.8 dB. Consequently the transmission coefficient requirement is met.

The defined phase shift of ports 3, 4 and 5 relative to port 2 should be -90°, -180° and -270° respectively. The difference of real values from defined values of phase shifts should ideally be zero. The difference from zero indicates the design error and this is implied as PE3, PE4 and PE5 for ports 3 to 5, respectively and illustrated in Figure 11. As clearly shown, the maximum error in this study is about 9 degrees which is acceptable for phase difference requirement.

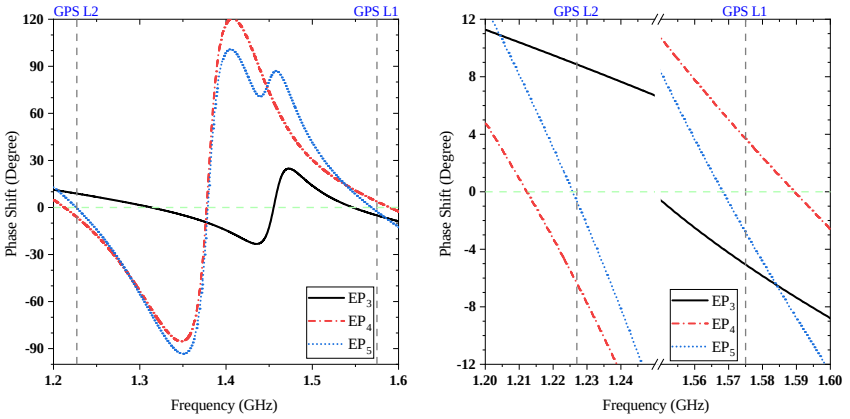

(a) General view (b) Magnified view

Figure 11: Phase shift of output ports relative to each other

The phase shift between the ports is created by a part of the transmission line. According to the following relationship, the phase shift is proportional to the physical length of the transmission line.

$$EL = \beta l = \frac{2\pi}{\lambda} l = \frac{2\pi f}{c} l = \frac{2\pi l}{c} f \tag{3.1}$$

where EL is the electrical length of the transmission line (which indicates the amount of phase shift of the transmission line) in $[rad]$, β states the Phase constant in $[rad/s]$, λ implies the wavelength in $[m]$, f is the frequency in $[Hz]$ and l is the physical length of the line in $[m]$. Since the electrical length of the line is proportional to the frequency, the transmission line cannot provide the condition of 270° phase shift at both frequencies. In practice, if the physical length of the line is set to provide electrical length of 4.71 radians (270°) at GPS L2=1.22 GHz, then at the frequency

of GPS L1=1.575 GHz, the electrical length of the line will be 6.08 radians (348°) and therefore error of 1.37 (78.5°) is occurred. Consequently, in this study, a coupler is used instead of the transmission line. By using a coupler, the relationship between the electrical length of the transmission line and the frequency is not necessarily linear, and therefore, with the right design, the phase shift can be almost the same at both frequencies as earlier shown in Figure 11.

The schematic of the designed feeding network and also the fabricated one is depicted in Figure 12 and Figure 13, respectively.

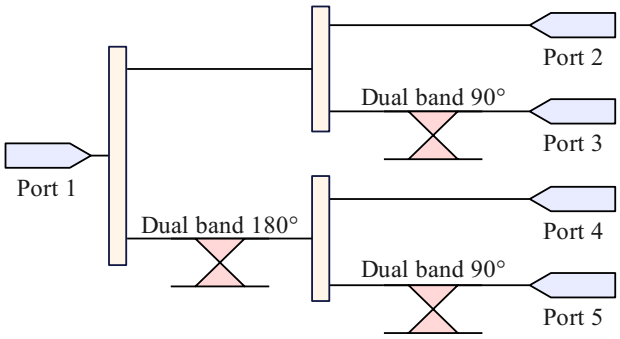

Figure 12: Schematic of feeding network

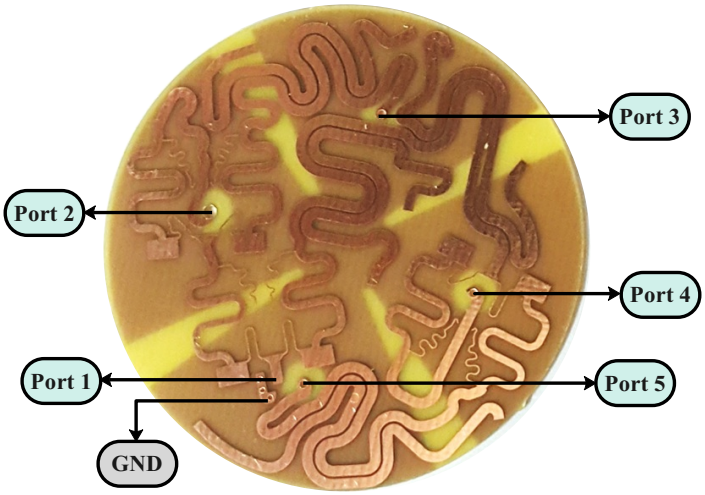

Figure 13: Fabricated Feeding Network

3.2 Antenna performance

In this investigation, a dual-band, low-cost, miniaturized microstrip antenna is designed for GNSS applications. The proposed antenna is able to operate at GPS L1 (1575 MHz) and L2 (1227 MHz), GLONASS G1 (1602 MHz) and G3 (1207 MHz), Galileo E1 (1589 MHz), E2 (1561 MHz) and E5b (1207 MHz) bands. Circular polarization is generated by creating circular slots on the patch, generating fractal sectors and also employing a four-fed network. Novel geometry, easy and low-cost fabrication and compact size are the main aspects of the designed antenna. The antenna size is 1548 mm^2 with the thickness of 2 mm. Results are expressed in terms of return loss, right hand electrical field and AR. The return loss versus frequency is shown in Figure 14. The proposed antenna has desirable band-width of 48 and 60 MHz at f_1 =1.227GHz (GPS L2) and f_2 =1.575GHz (GPS L1), respectively.

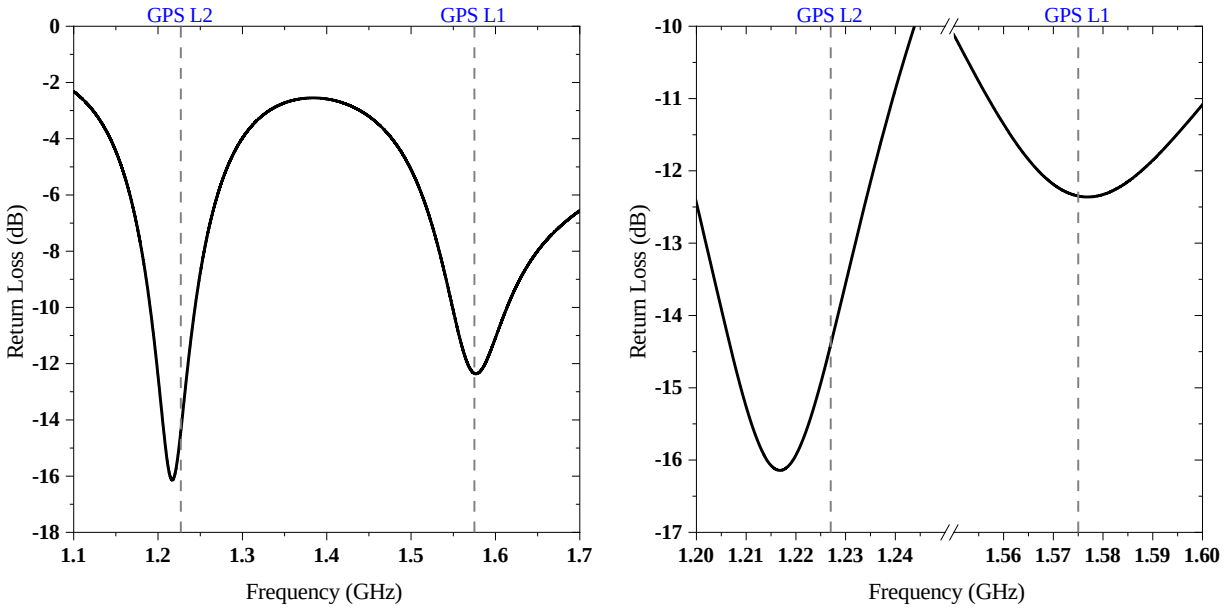

(a) General view (b) Magnified view

Figure 14: Return loss curve

The axial ratio of the proposed antenna is plotted in Figure 15. As it is clearly shown, at more than 66°, the AR is below $3dB$ which is an indication of the pure right-handed circular polarization.

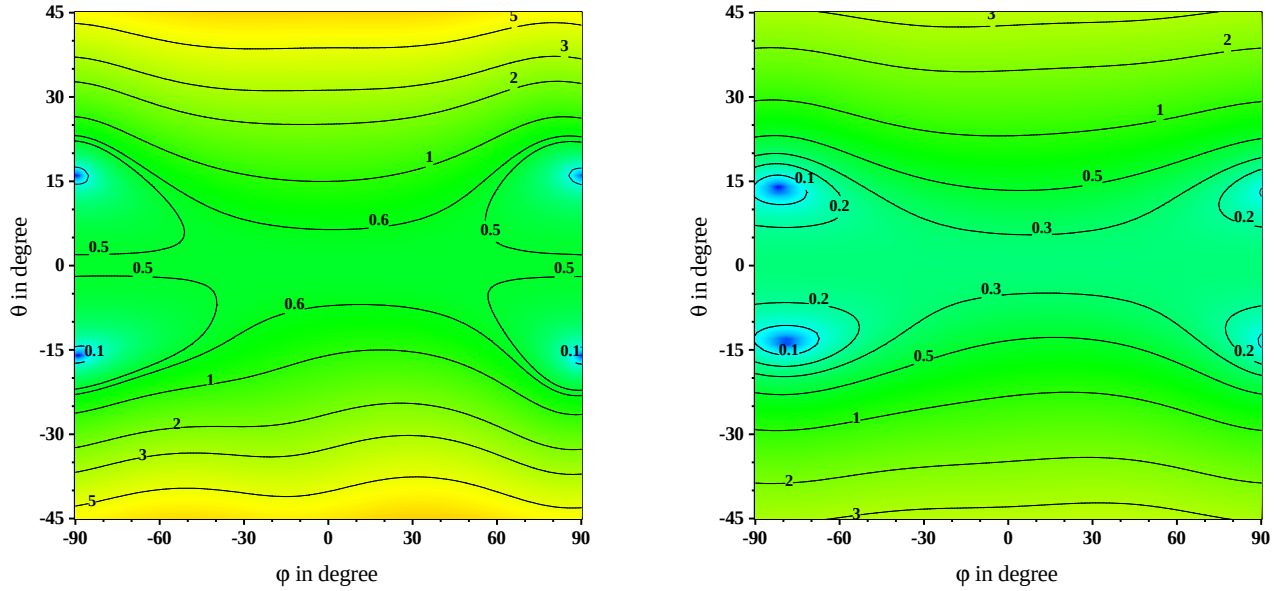

(a) GPS L1 frequency (b) GPS L2 frequency

Figure 15: Antenna Axial Ratio

4 Conclusion

In this study a low-cost, miniaturized, dual-band microstrip antenna is proposed. The resonant frequencies are GPS L1=1.575 GHz and L2=1.227 GHz. Multiple-feed relations are driven to analyze situations leads to pure circular

polarization. Finally the four-feed antenna performance is evaluated via numerical simulation. The following results are obtained.

- For a symmetric n-feed antenna, setting the temporal phase shift as the negative value of spatial phase shift $\left(-\frac{2\pi}{n}\right)$, leads to pure circular polarization regardless the properties of electrical field.

- The electric field of first feed with same value of x and y component and also 90° phase shift between them increase the right-hand circular polarization gain.

- In the dual-band 4-feed Antenna, the phase shift requirement at both resonant frequency is met, using coupler device.

- The proposed antenna has desirable performance with band-width of 48 MHz and 60 MHz and also front to back ratio of 10.4 dB and 40 dB at GPS L1 and GPS L2, respectively. The AR at both frequencies is more than 66°.

References

[1] K. Agarwal, Nasimuddin, and A. Alphones, *Triple-band compact circularly polarised stacked microstrip antenna over reactive impedance meta-surface for GPS applications*, IET Microwaves Antennas Propag. **8** (2014), no. 13, 1057–1065.

[2] F. Bilotti and C. Vegni, *Design of high-performing microstrip receiving GPS antennas with multiple feeds*, IEEE Antennas Wireless Propag. Lett. **9** (2010), 248–251.

[3] H. Chen, Y. Wang, Y. Lin, Ch. Lin, and Sh. Pan, *Microstrip-Fed Circularly Polarized Square-Ring Patch Antenna for GPS Applications*, IEEE Trans. Antennas Propag. **57** (2009), no. 4, 1264–1267.

[4] J. Chen, K. Tong, A. Al-Armaghany, and J. Wang, *A dual-band dual-polarization slot patch antenna for GPS and wi-fi applications*, IEEE Antennas Wireless Propag. Lett. **15** (2016), 406–409.

[5] N.K. Darimireddy, R.R. Ramana, N. Rajasekhar, and P. Srinivasa Rao, *Rhombic slotted pentagonal patch antenna for GPS applications*, 2018 IEEE Indian Conf. Antennas Propog. (InCAP), IEEE, 2018, pp. 1–4.

[6] C.D. Erbas, *Annular ring microstrip patch antennas with slots in patch and ground plane for GSM-1800 and radio navigation*, 8th Int. Conf. Electric. Electron. Engin. (ICEEE), IEEE, 2021, pp. 305–308.

[7] F.B. Gross, *Smart antennas for wireless communications with MATLAB*, McGraw-Hill Professional, 2005.

[8] C.E. Guan and T. Fujimoto, *Polarization-sense reconfigurable circular polarized antenna*, 2021, pp. 719–720.

[9] S.J. Jeong, *Compact circularly polarized antenna with a capacitive feed for GPS/GLONASS applications*, ETRI J. **34** (2012), no. 5, 767–770.

[10] E.K. Kaivanto, M. Berg, E. Salonen, and P. De Maagt, *Wearable circularly polarized antenna for personal satellite communication and navigation*, IEEE Trans. Antennas Propag. **59** (2011), no. 12, 4490–4496.

[11] S. Komeylian and S. Komeylian, *Deploying an OFDM physical layer security with high rate data for 5G wireless networks*, IEEE Canad. Conf. Electric. Comput. Engin. (CCECE), vol. 2020-Augus, IEEE, 2020, pp. 1–7.

[12] K.Y. Lam, K. Luk, K.F. Lee, H. Wong, and K.B. Ng, *Small circularly polarized U-slot wideband patch antenna*, IEEE Antennas Wireless Propag. Lett. **10** (2011), 87–90.

[13] Zh. Ma, J. Chen, P. Chen, and Y. F. Jiang, *Design of planar microstrip ultrawideband circularly polarized antenna loaded by annular-ring slot*, Int. J. Antennas Propag. **2021** (2021), 1–10.

[14] P.K. Malik, P. Kumar, S. Kumar, and D. Singh, *Smart Antennas: Latest Trends in Design and Application*, Advances in Computing Communications and Informatics, vol. 2, Bentham Science Publishers, 2022.

[15] P.K. Malik, S. Padmanaban, and J.B. Holm-Nielsen, *Microstrip Antenna Design for Wireless Applications*, CRC Press, New York, 2021.

[16] E.A. Marranghelli, G. Ramon Lopez La Valle, and P.A. Roncagliolo, *A spatial signal processing review for practical GNSS antenna arrays*, IEEE Bienn. Cong. Argentina (ARGENCON), IEEE, jun 2018, pp. 1–8.

[17] B.R. Perli and A.M. Rao, *Analysis of a compact 4-shaped annular ring ultra wideband antenna using characteristic modes*, Int. J. Electron. Telecommun. **68** (2022), no. 2, 229–235.

[18] Prachi and T.K. Mandal, *Dual frequency millimeter-wave perturbed ring patch antenna array for 5G applications*, IETE J. Res. (2021), 1–11.

[19] M. Sahal and V.N. Tiwari, *Review of circular polarization techniques for design of microstrip patch antenna*, Proc. Int. Conf. Recent Cognizance Wireless Commun. Image Process. (Nitin Afzalpulkar, Vishnu Srivastava, Ghanshyam Singh, and Deepak Bhatnagar, eds.), Springer India, New Delhi, 2016, pp. 663–669.

[20] M. Shakeeb, *Circularly polarized microstrip antenna*, Ph.D. thesis, Concordia University, 2010.

[21] Y.A. Sheikh, K.N. Paracha, S. Ahmad, A.R. Bhatti, A.D. Butt, and S.K.A. Rahim, *Analysis of compact dual-band metamaterial-based patch antenna design for wearable application*, Arab. J. Sci. Engin. **47** (2022), no. 3, 3509–3518.

[22] J. Sze and W. Chen, *Axial-ratio-bandwidth enhancement of a microstrip-line-fed circularly polarized annular-ring slot antenna*, IEEE Trans. Antennas Propag. **59** (2011), no. 7, 2450–2456.

[23] J. Zhao, Zh. Zhang, Y. Li, G. Fu, and Sh. Gong, *Wideband patch antenna with stable high gain and low cross-polarization characteristics*, Prog. Electromag. Res. Lett. **45** (2014), no. January, 35–38.